

Spin-orbit coupling and Kondo resonance in Co adatom on Cu(100) surface: DFT+ED study

A. B. Shick and M. Tchaplianka

*Institute of Physics, Czech Academy of Science, Na Slovance 2, CZ-18221 Prague, Czech Republic**

A. I. Lichtenstein

*Institute of Theoretical Physics, University of Hamburg, 20355 Hamburg, Germany and
European X-Ray Free-Electron Laser Facility, Holzkoppel 4, 22869 Schenefeld, Germany*

(Dated: October 4, 2022)

We report density functional theory plus exact diagonalization of the multi-orbital Anderson impurity model calculations for the Co adatom on the top of Cu(001) surface. For the Co atom d -shell occupation $n_d \approx 8$, a singlet many-body ground state and Kondo resonance are found, when the spin-orbit coupling is included in the calculations. The differential conductance is evaluated in a good agreement with the scanning tunneling microscopy measurements. The results illustrate the essential role which the spin-orbit coupling is playing in a formation of Kondo singlet for the multi-orbital impurity in low dimensions.

I. INTRODUCTION

The electronic nanometer scaled devices require the atomistic control of their behaviour governed by the electron correlation effects. One of the most famous correlation phenomena is the Kondo effect originating from screening of the local magnetic moment by the Fermi sea of conduction electrons, and resulting in a formation of a singlet ground state [1]. Historically the Kondo screening was detected as a resistance increase below a characteristic Kondo temperature T_K in dilute magnetic alloys [2]. Recent advances in scanning tunneling microscopy (STM) allowed observation of the Kondo phenomenon on the atomic scale, for atoms and molecules at surfaces [3, 4]. In these experiments, an enhanced conductance near the Fermi level (E_F) is found due to the formation of a sharp Abrikosov-Suhl-Kondo [5–7] resonance in the electronic density of states (DOS).

One case of the Kondo effect the most studied experimentally and theoretically is that of a Co adatom on the metallic Cu substrate [3, 8–10]. The experimental STM spectra display sharp peaks at zero bias, or so called "zero-bias" anomalies, similar to the Fano-resonance [11] found in the atomic physics, which are associated with the Kondo resonance. The theoretical description of the Kondo screening in multiorbital d manifold is difficult since the whole d shell is likely to play a role. Very recently, theoretical electronic structure of the Co atom on the top of Cu(100) was considered [10] using numerically exact continuous-time quantum Monte-Carlo (CTQMC) method [12] to solve the multiorbital single impurity Anderson model [13] (SIAM) together with the density-functional theory [14] as implemented in the W2DYNAMICS package [15, 16]. However, the spin-orbit coupling (SOC) was neglected. The peak in the DOS at

E_F was obtained in these calculations, and was interpreted as a signature of the Kondo resonance.

Alternative interpretation was proposed [17] which is based on the spin-polarized time-dependent DFT in conjunction with many-body perturbation theory. These authors claim that the "zero-bias" anomalies are not necessarily related to the Kondo resonance, and are connected to interplay between the inelastic spin excitations and the magnetic anisotropy. Thus the controversy exists concerning the details of the physical processes underlying the Kondo screening in Co@Cu(100). In this work, we revisit Co@Cu(100) case making use of the combination of DFT with the exact diagonalization of multiorbital SIAM (DFT+ED) including SOC. We demonstrate that SOC plays crucial role in formation of the singlet ground state (GS) and the Kondo resonance.

II. METHODOLOGY: DFT + EXACT DIAGONALIZATION

The exact diagonalization (ED) method is based on a numerical solution of the multi-orbital Anderson impurity model (AIM) [13]. The continuum of the bath states is discretized. The five d -orbitals AIM with the full spherically symmetric Coulomb interaction, a crystal field (CF), and SOC is written as,

$$\begin{aligned}
 H = & \sum_{km\sigma} \epsilon_{km} b_{km\sigma}^\dagger b_{km\sigma} + \sum_{m\sigma} \epsilon_d d_{m\sigma}^\dagger d_{m\sigma} \\
 & + \sum_{mm'\sigma\sigma'} (\xi \mathbf{l} \cdot \mathbf{s} + \Delta_{\mathbf{CF}})_{mm'}^\sigma d_{m\sigma}^\dagger d_{m'\sigma'}^\dagger \\
 & + \sum_{km\sigma} \left(V_{km} d_{m\sigma}^\dagger b_{km\sigma} + h.c. \right) \\
 & + \frac{1}{2} \sum_{mm'm''m'''\sigma\sigma'} U_{mm'm''m'''} d_{m\sigma}^\dagger d_{m'\sigma'}^\dagger d_{m''\sigma''} d_{m'''\sigma'''}
 \end{aligned} \tag{1}$$

The impurity-level position ϵ_d which yield the desired $\langle n_d \rangle$, and the bath energies ϵ_{km} are measured from the

*Electronic address: shick@fzu.cz

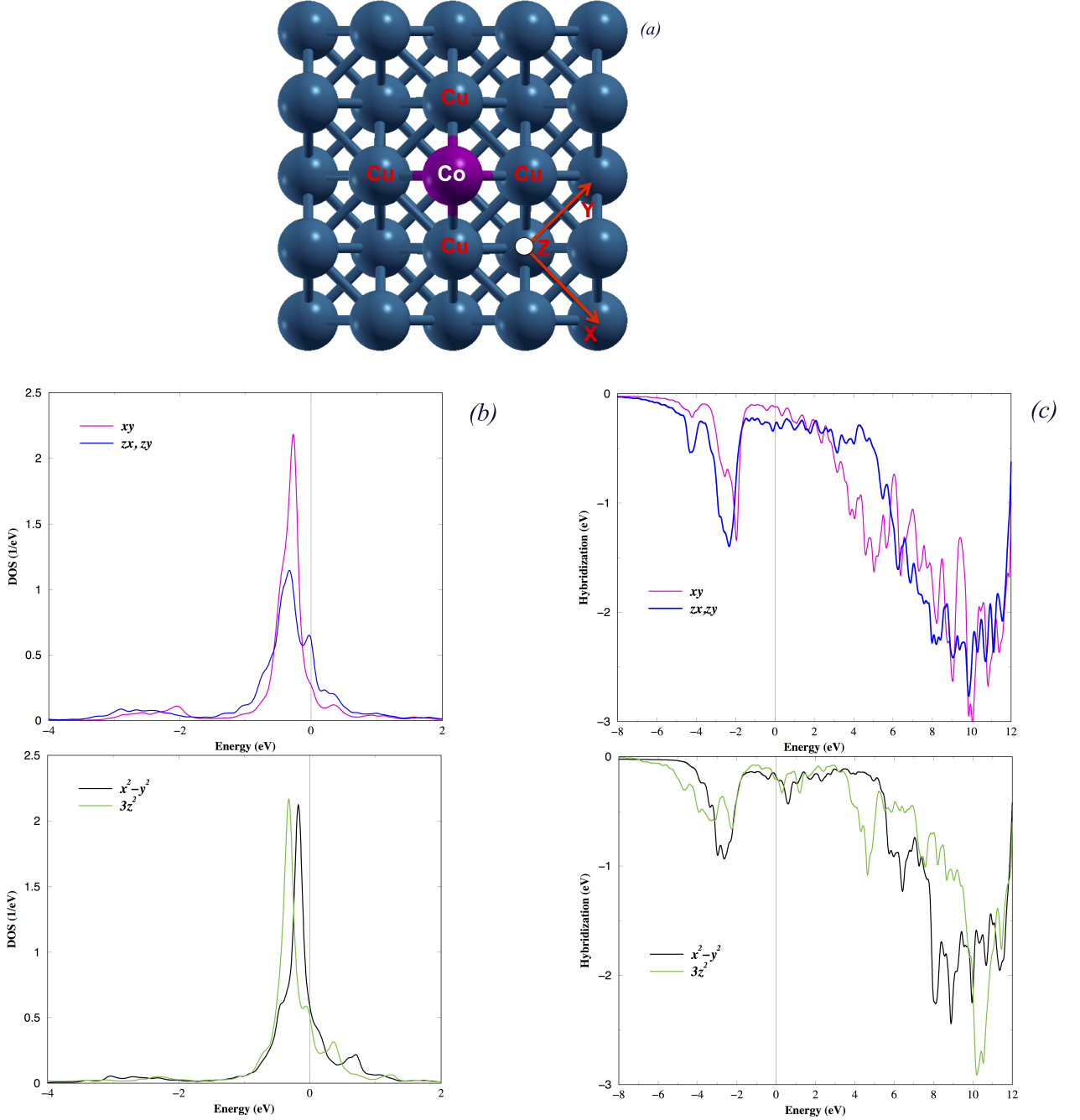


FIG. 1: The ball model (top view) for Co@4Cu] supercell. The specific choice of the Cartesian reference frame is show. With this choice, the local Green's function without SOC becomes diagonal in the basis of cubic harmonics $m = \{xz, yz, xy, x^2 - y^2, 3z^2 - r^2\}$ (a); orbitally resolved DOS (b); orbitally resolved hybridization $\text{Im } \Delta$ (c) for the Co adatom on Cu(001),

chemical potential μ , that was set to zero. The SOC ξ parameter specifies the strength of the spin-orbit coupling, whereas Δ_{CF} matrix describes CF acting on the impurity. The hybridization V_{mk} parameters describe the coupling of substrate to the impurity orbitals. These parameters are determined from DFT calculations, and their particular choice will be described below.

The last term in Eq.(1) represents the Coulomb in-

teraction. The Slater integrals $F_0 = 4.00$ eV, $F_2 = 7.75$ eV, and $F_4 = 4.85$ eV are used for the Coulomb interaction [9, 10]. They correspond to the values for the Coulomb $U = 4$ eV and exchange $J = 0.9$ eV for Co which are in the ballpark of commonly accepted U and J for transitional 3d-metals.

The DFT calculation were performed on a supercell of four Cu(100) layers, and the Co adatom followed by four

empty Cu layers modeling the vacuum. Fig. 1A shows ball model of the Co@[4Cu₈] supercell employed for the adsorbate atop of Cu. The structure relaxation was performed employing the VASP method [18] together with the generalized gradient approximation (GGA) to spin-polarized DFT without SOC. The adatom-substrate distance as well as the atomic positions within two Cu(100) layers underneath were allowed to relax. The relaxed distance between the Co adatom in a fourfold hollow position and the first Cu substrate layer of 2.91 *a.u.* is in a good agreement with previously reported value of 2.87 *a.u.* [10].

In order to obtain the bath parameters in the AIM Hamiltonian Eq.(1) we make use of the recipes of the dynamical mean-field theory (DMFT) [19, 20], and employ the DFT(LDA) local Green's function $G_0(z)$

$$[G_0(z)]_{\gamma_1\gamma_2} = \frac{1}{V_{\text{BZ}}} \int_{\text{BZ}} d^3k [z + E_F - H_{\text{DFT}}(\mathbf{k})]_{\gamma_1\gamma_2}^{-1}, \quad (2)$$

calculated with help of the full-potential linearized augmented plane wave method (FLAPW) [21, 22], in order to define the parameters for the Eq.(1). Here, the energy z is counted from the Fermi energy E_F , and the index $\gamma \equiv lm\sigma$ marks the d -orbitals in the MT-sphere of the Co adatom. Note that the non-spin-polarised LDA is used to extract the hybridization function $\Delta(z)$. The orbitally resolved density of states (DOS) together with the hybridization function $\text{Im} \Delta$ are shown in Fig. 1B,C. They are compatible with the results of Ref. [23]. Further details of constructing the discrete bath model are given in Appendix A. The fitted bath parameters are shown in Table IV. These parameters are used to build the AIM Hamiltonian Eq.(1).

The SOC parameter $\xi = 0.079$ eV is taken from LDA calculations in a standard way,

$$\xi = \int_0^{R_{\text{MT}}} dr r \frac{1}{2(Mc)^2} \frac{dV(r)}{dr} (u_l(r))^2,$$

making use of the radial solutions u_l of the Kohn-Sham-Dirac scalar-relativistic equations [24], the relativistic mass $M = m + (E_l - V(r))/2c^2$ at an appropriate energy E_l , and the radial derivative of spherically-symmetric part of the LDA potential.

III. RESULTS AND DISCUSSION

The total number of electrons N , and the d -shell occupation are controlled by the ϵ_d parameter. It has a meaning of the chemical potential $\mu = -\epsilon_d$ in Eq. (1). In DMFT it is quite common to use $\mu = V_{dc}$, the spherically-symmetric double-counting which has a meaning of the mean-field Coulomb energy of the d -shell, and to use standard (AMF) $V_{dc} = (U/2 n_d + \frac{2l}{2(2l+1)} (U - J) n_d)$ [27] form, or the fully localized limit (FLL) $V_{dc} = (U - J)/2 (n_d - 1)$ [28]. Since precise definition of n_d depends

on the choice of the localized basis, we adopt a strategy of Ref. [9], and consider a value of μ as a parameter.

A. Co in the bulk Cu

At first, we consider the Co impurity in the bulk Cu making use of the CoCu₁₅ supercell model. DFT+ED calculations for different values of μ in a comparison with previous DFT+CTQMC results [9] are described in details in Ref. [25]. Here, we adjust the value of μ in order to have the Co atom d -shell occupation $n_d \approx 8$. This valence of Co in the bulk Co follows from DFT calculations [9, 25].

Without SOC we found that the value of $\mu = 27.4$ corresponds to the $n_d \approx 8$ occupation. The GS solution without SOC (see Table I) is the $|\Omega\rangle_{N=30}$ singlet, and the excited triplet is ≈ 0.4 eV higher in the energy. Note that each eigenstate $|\Omega\rangle_N$ of Eq.(1) corresponds to an integer N occupation (d -shell + bath) since \hat{N} commutes with Hamiltonian Eq.(1). For each $|\Omega\rangle$, the probabilities to find the atomic eigenstates $|n\rangle$ with integer occupation d^n , $P_n = \langle n|\Omega\rangle\langle\Omega|n\rangle$, and the d -shell occupation $n_d = \sum_n P_n n d^n$.

The corresponding density of d -states (DOS) [1]:

$$A(\epsilon) = -\frac{1}{\pi Z} \text{Im} \sum_{\gamma, \alpha, \beta} \frac{\langle \Omega_\alpha | c_\gamma | \Omega_\beta \rangle \langle \Omega_\beta | c_\gamma^\dagger | \Omega_\alpha \rangle}{\epsilon + i\delta + E_\alpha - E_\beta} [e^{-\beta E_\beta} + e^{-\beta E_\alpha}] \quad (3)$$

where the α, β run over the eigenstates of Hamiltonian Eq.(1), $\gamma \equiv \{m, \sigma\}$ marks the single particle spin-orbital, is shown in Fig. 2a, with the peak in DOS very near E_F .

The expectation values of the total $\langle \Omega | J_z | \Omega \rangle$, orbital $\langle \Omega | L_z | \Omega \rangle$, and spin $\langle \Omega | S_z | \Omega \rangle$ angular momenta for the $|\Omega\rangle_{N=30}$ singlet GS and the excited triplet are shown in Table I. They correspond to a solution of the Kondo model for localized $S = \frac{1}{2}$ anti-ferromagnetically coupled to a single band of conduction electrons [26]. Together with the Kondo peak in DOS (cf. Fig. 2a) our DFT+ED solution corresponds to the Kondo singlet state.

When SOC is included, and the spin is not a good quantum number, there are minor changes in the character for $\mu = 27.5$ ($n_d \approx 8$), the GS solution $|\Omega\rangle_{N=30}$: GS is a singlet, and the excited triplet consists of an effective $|J=1, J_z=-1, 0, 1\rangle$ degenerate states which are ≈ 0.5 eV higher in the energy. The DOS has a peak in DOS very near E_F . It is seen that weak $3d$ -shell SOC plays no essential role for the Co impurity in the Cu host. These calculations show that our DFT+ED approach is capable to reproduce the Kondo singlet for Co in the bulk Cu for $n_d = 8$, in agreement with conclusions of DFT+CTQMC [9]. Also, in agreement with commonly accepted point of view [32], we show that the presence of SOC does not lead to essential modification of a Kondo model.

TABLE I: The total number of particles (d -shell + bath) N , the expectation values $\langle \Omega | J_z | \Omega \rangle$, $\langle \Omega | L_z | \Omega \rangle$, $\langle \Omega | S_z | \Omega \rangle$ angular momenta, non-zero probabilities P_{d^n} to find the atomic eigenstates $|n\rangle$ with integer occupation d^n for GS and low-energy excitation energies for different values of μ .

without SOC							
	Energy (eV)	J_z	L_z	S_z	P_{d^7}	P_{d^8}	P_{d^9}
$\mu=27.4$ eV, $n_d=8.05$							
$N=30$	-148.5822	0.	0.	0.	0.20	0.51	0.26
	-148.1014	0.53	0	0.53	0.22	0.55	0.20
	-148.1014	0	0	0	0.22	0.55	0.20
	-148.1014	-0.53	0	-0.53	0.22	0.55	0.20
with SOC							
	Energy (eV)	J_z	L_z	S_z	P_{d^7}	P_{d^8}	P_{d^9}
$\mu=27.5$ eV, $n_d=7.99$							
$N=30$	-149.4028	0.	0.	0.	0.19	0.51	0.27
	-148.9296	0.94	0.49	0.45	0.21	0.55	0.21
	-148.9296	0.	0.	0.	0.21	0.55	0.21
	-148.9296	-0.94	-0.49	-0.45	0.21	0.55	0.21

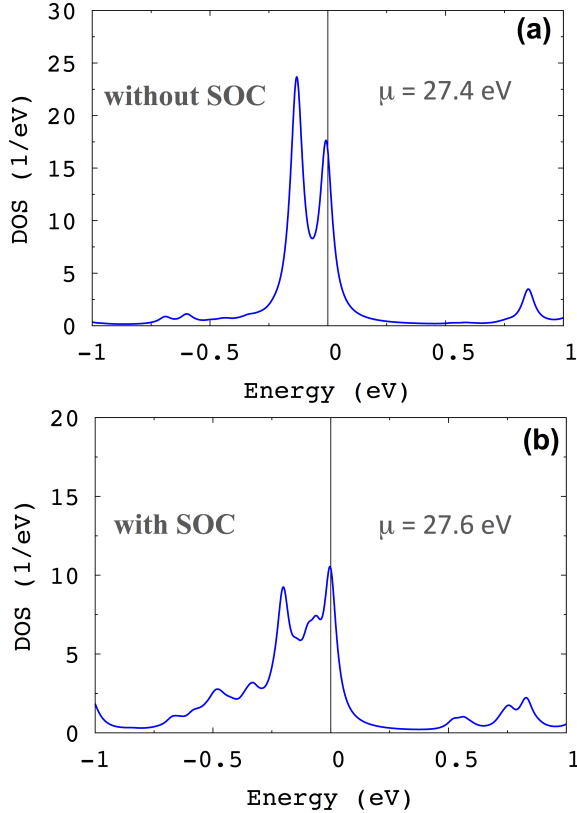


FIG. 2: DOS for the Co in the bulk Cu without SOC for $\mu=27.4$ eV (a), and with SOC for $\mu=27.5$ eV (b).

B. Co on Cu(001)

Now we turn to a salient aspect of our investigation, the Co adatom on Cu(001) surface. Considering a value of μ as a parameter, we analyse the ground state (GS) of

Eq.(1) with and without SOC for different values of μ . Making use of grand-canonical averages at low temperature $k_B T = \beta^{-1} = (1/500)$ eV (20K) we calculate the expectation values of total number of electrons (d -shell + bath) $\langle N \rangle$, the charge fluctuation $(\langle N^2 \rangle - \langle N \rangle^2)^{\frac{1}{2}}$ near the GS, the expectation values of spin (S), orbital (L) and total spin-orbital (J) moments, and show them in Table II together with the d -shell occupation n_d for the GS, and corresponding P_n probabilities, with and without SOC.

For the values of $\mu = 26$ eV and 27 eV, the GS is the eigenstate $|\Omega\rangle_{N=26}$, and is a combination of d^7 ($P_{d^7} \approx 0.3$) and d^8 ($P_{d^8} \approx 0.6$). These state have a non-integer n_d occupation due to hybridization of the atomic d -states with the substrate. Nevertheless, the $(\langle N^2 \rangle - \langle N \rangle^2)^{\frac{1}{2}} \approx 0$ pointing on the absence of charge fluctuations. The S values lie between of $S = 3/2$ (the atomic d^7 , 4F), and $S = 1$ (the atomic d^8 , 3F), while the L is close to the atomic $L = 3$. The expectation values of the z -axis projections of the total $\langle \Omega | J_z | \Omega \rangle$, orbital $\langle \Omega | L_z | \Omega \rangle$, and spin $\langle \Omega | S_z | \Omega \rangle$ angular momenta for GS and low-energy excitation energies for $\mu = 27.0$ eV are shown in Tab. III. It is seen that without SOC the GS can be interpreted as $S = 1$ -like triplet. For $\mu = 28$ eV, the GS is the eigenstate $|\Omega\rangle_{N=27}$, and the contributions of d^7 ($P_{d^7} \approx 0.1$) and d^8 ($P_{d^8} \approx 0.5$) are reduced while d^9 , 2D ($P_{d^9} \approx 0.3$) is increased. Again, there are no charge fluctuations near the GS. This GS looks similar to $S = 1/2$ doublet (see Tab. III).

When the SOC is included, for the values of $\mu = 26$ eV, 27 eV the eigenstate $|\Omega\rangle_{N=26}$ is split to the lowest energy singlet plus excited doublet (see Tab. III). These states approximately correspond to $|J = 1, J_z\rangle$ eigenstates of the effective Hamiltonian [29],

$$\hat{H}_{MA} = D\hat{J}_z^2 + E(\hat{J}_x^2 - \hat{J}_y^2), \quad (4)$$

with the uniaxial magnetic anisotropy $D \approx 4.5$ meV, and $E = 0$. For $\mu = 28$ eV, the GS remains $|\Omega\rangle_{N=27}$ doublet.

The corresponding densities of d -states (DOS) for the values of $\mu = 26$ eV, 27 eV, 28 eV are shown in Appendix B Fig. 5. There are similarities in the DOS with and without SOC: no peak in DOS in a close vicinity of E_F . For these values of μ and without SOC there are no singlet GS, and no Kondo resonances in the DOS. In a presence of SOC, even their GS become singlets for $\mu = 26, 27$ eV, no Kondo peaks are formed. For $\mu = 28$ eV the GS solution remains a doublet without Kondo resonance in the DOS.

Since the change in the GS with the variation of μ between 27 eV and 28 eV is observed, we further adjust the values of μ in order to keep the same $n_d \approx 8$ without and with the SOC. In case of $\mu=27.4$ eV and without the SOC, we obtain a non-integer $\langle N \rangle=26.55$, non-zero $(\langle N^2 \rangle - \langle N \rangle^2)^{\frac{1}{2}} \approx 0.5$ charge fluctuations, and $n_d=7.93$. This solution is formally close to “ d^8 ” state but actually a combination of d^7 ($P_{d^7} \approx 0.21$), d^8 ($P_{d^8} \approx 0.58$), and d^9 ($P_{d^9} \approx 0.18$) atomic states (see Tab. II).

TABLE II: The chemical potential μ (eV), the occupation $\langle N \rangle$, fluctuation $(\langle N^2 \rangle - \langle N \rangle^2)^{\frac{1}{2}}$, n_d occupation, non-zero probabilities P_{d^n} to find the atomic eigenstates $|n\rangle$ with integer occupation d^n , spin, orbital and total moments of the impurity d -shell for different values of μ . Grand-canonical averages are at low temperature $k_B T = \beta^{-1} = (1/500)$ eV.

without SOC										
μ (eV)	$\langle N \rangle$	$(\langle N^2 \rangle - \langle N \rangle^2)^{\frac{1}{2}}$	n_d	P_{d^6}	P_{d^7}	P_{d^8}	P_{d^9}	S	L	J
26	26.00	0.00	7.57	0.05	0.34	0.56	0.03	1.10	3.07	3.40
27	26.00	0.01	7.74	0.03	0.27	0.62	0.08	1.03	3.01	3.32
27.4	26.55	0.50	7.93	0.02	0.21	0.58	0.18	0.94	2.87	3.15
28	27.00	0.00	8.17	0.01	0.14	0.51	0.33	0.82	2.68	2.91
with SOC										
μ (eV)	$\langle N \rangle$	$(\langle N^2 \rangle - \langle N \rangle^2)^{\frac{1}{2}}$	n_d	P_{d^6}	P_{d^7}	P_{d^8}	P_{d^9}	S	L	J
26	26.00	0.00	7.58	0.05	0.34	0.57	0.04	1.09	3.07	3.89
27	26.00	0.00	7.75	0.03	0.26	0.62	0.08	1.03	3.01	3.82
27.6	26.38	0.48	7.96	0.02	0.20	0.58	0.19	0.93	2.86	3.51
28	27.00	0.00	8.17	0.01	0.14	0.51	0.33	0.82	2.68	3.16

TABLE III: The total number of particles (d -shell + bath) N , the expectation values $\langle \Omega | J_z | \Omega \rangle$, $\langle \Omega | L_z | \Omega \rangle$, $\langle \Omega | S_z | \Omega \rangle$ angular momenta, non-zero probabilities P_{d^n} to find the atomic eigenstates $|n\rangle$ with integer occupation d^n for GS and low-energy excitation energies for different values of μ .

without SOC							
	Energy (eV)	J_z	L_z	S_z	P_{d^7}	P_{d^8}	P_{d^9}
$\mu=27.0$ eV							
$N=26$	-142.2319	0.0	0.0	0.0	0.27	0.62	0.08
	-142.2319	0.90	0.0	0.90	0.27	0.62	0.08
	-142.2319	-0.90	0.0	-0.90	0.27	0.62	0.08
$\mu=27.4$ eV							
$N=26$	-145.3478	0.00	0.0	0.00	0.23	0.61	0.13
	-145.3478	0.81	0.0	0.81	0.23	0.61	0.13
	-145.3478	-0.81	0.0	-0.81	0.23	0.61	0.13
$N=27$	-145.3490	0.57	0.0	0.57	0.19	0.55	0.23
	-145.3490	-0.57	0.0	-0.57	0.19	0.55	0.23
$\mu=28.0$ eV							
$N=27$	-150.1992	0.53	0.0	0.53	0.14	0.51	0.33
	-150.1992	-0.53	0.0	-0.53	0.14	0.51	0.33
with SOC							
	Energy (eV)	J_z	L_z	S_z	P_{d^7}	P_{d^8}	P_{d^9}
$\mu=27.0$ eV							
$N=26$	-142.3054	0.00	0.0	0.00	0.26	0.62	0.08
	-142.3009	1.48	0.91	0.57	0.26	0.62	0.08
	-142.3009	-1.48	-0.91	-0.57	0.26	0.62	0.08
$\mu=27.6$ eV							
$N=26$	-146.9950	0.00	0.0	0.00	0.21	0.61	0.16
	-146.9912	1.10	0.70	0.40	0.21	0.61	0.16
	-146.9912	-1.10	-0.70	-0.40	0.21	0.61	0.16
$N=27$	-146.9931	1.43	0.95	0.48	0.18	0.54	0.26
	-146.9931	-1.43	-0.95	-0.48	0.18	0.54	0.26
$\mu=28.0$ eV							
$N=27$	-150.2373	1.37	0.91	0.45	0.14	0.51	0.33
	-150.2373	-1.37	-0.91	-0.45	0.14	0.51	0.33

There is a peak near E_F in the DOS shown in Fig. 3(a). Note that similar peak in DOS was obtained in CTQM calculations [10] without SOC with the same choice of the Coulomb- U and the exchange- J , and $n_d=8$ very close to our calculations. In Ref. [10] it is interpreted as a spectral

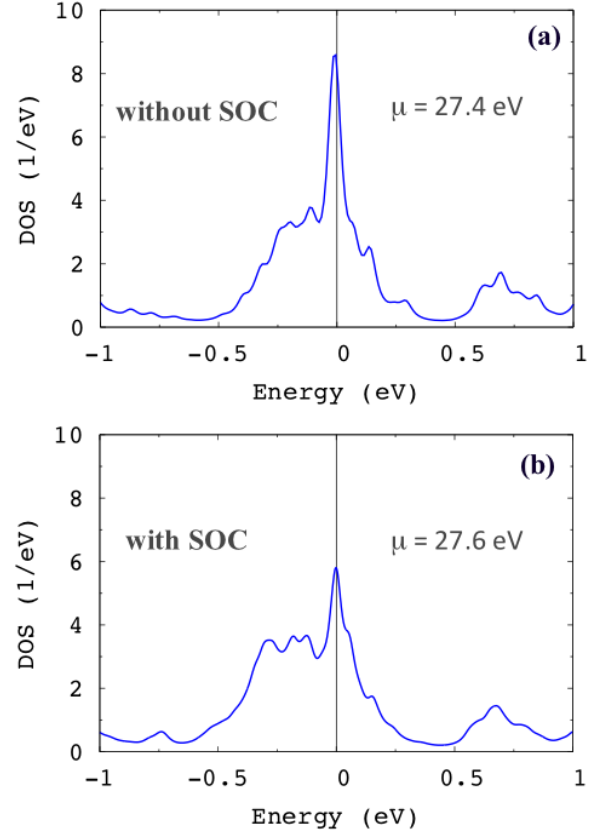


FIG. 3: DOS for the Co@Cu(001) as a function of $\mu=27.5$ eV without SOC (a), and with SOC (b), $\mu=27.4$ eV without SOC (c), and 27.6 eV with SOC (d).

signature of the Kondo effect. As follows from Eq. (3) the presence of such a peak signals the (quasi)-degeneracy of the eigenvalues E_N , and $E_{N\pm 1}$. These are the $|\Omega\rangle_{N=27}$ doublet and $|\Omega\rangle_{N=26}$ triplet states which differ in the energy by 1.2 meV (see Tab. III), with the doublet GS $|\Omega\rangle_{N=27}$. Since there is no singlet GS, the DOS peak at

E_F is not a Kondo resonance, and signals the presence of valence fluctuations [29].

When the SOC is included, and with $\mu=27.6$ eV, there is a non-integer $\langle N \rangle=26.38$, with non-zero charge fluctuations $(\langle N^2 \rangle - \langle N \rangle^2)^{\frac{1}{2}} \approx 0.5$, and $n_d=7.96$ (see Tab. II). Again, the DOS has a peak at E_F which is shown in Fig. 3(d). In this case, the (quasi)-degeneracy occurs between the singlet $|\Omega\rangle_{N=26}$ state being 1.9 meV lower in the energy than the $|\Omega\rangle_{N=27}$ doublet (see Tab. III). The DOS peak at E_F due to $|\Omega\rangle_{N=26}$ -to- $|\Omega\rangle_{N=27}$ transition can be interpreted as a Kondo resonance.

For the singlet GS we can use the renormalized perturbation theory [13] in order to estimate the Kondo temperature,

$$T_K = -\frac{\pi}{4} Z \text{Im}[\Delta(E_F)], \quad (5)$$

where

$$\hat{Z} \approx \frac{\text{Tr}[(\hat{I} - d \text{Re}[\Sigma(\epsilon)])/d\epsilon(E_F)]^{-1} A(E_F)}{\text{Tr}[A(E_F)]}$$

is a quasiparticle weight, and $A(E_F)$ is the DOS matrix from Eq.(3). We obtain $Z=0.097$, and corresponding $T_K = 0.019$ eV (≈ 220 K). It exceeds the experimental estimate $T_K = 88$ K [3] of the Kondo scale. Indeed, Eq. (5) serves as an order of magnitude estimate of T_K .

The scanning tunnelling spectroscopy measures the differential conductance $\mathcal{G}(V)$ through the adatom, and allows to probe the DOS. Comparison between the experimental and theoretical $\mathcal{G}(V)$ is the most direct way to distinguish between different theoretical approximations and to identify the most appropriate theoretical approach. Experimentally $\mathcal{G}(V)$ of Co@Cu(100) was studied in Ref. [3]. Observed step-like behaviour was interpreted in terms of interference between two tunnelling channels: (i) tunnelling to the d -DOS shown in Fig. 5, and (ii) tunnelling into the conduction electrons of the Cu substrate modified by the presence of the Co adatom. At the low bias, the differential conductance is then expressed [30] in the basis of cubic harmonics as,

$$\mathcal{G}(\omega) \sim \sum_m (1 + \Gamma_m((1 - q_m^2) \text{Im}[G_m(\omega)] + 2q_m \text{Re}[G_m(\omega)])) \quad (6)$$

where $G_m(\equiv G_{mm})$ is a Green's function of the Hamiltonian Eq.(1), $\Gamma_m \equiv -\text{Im}[\Delta_m(E_F)]$ is a hybridization between the d -level m and the substrate shown in Fig. 1C, and q_m is a Fano parameter. For the strongly localized Co adatom d -orbitals [31],

$$q_m \approx -\text{Re}[G_{0,m}(E_F)]/\text{Im}[G_{0,m}(E_F)].$$

The calculated $\mathcal{G}(V)$ is in a fair quantitative agreement with the experimental data [3]. Note that our results seem to agree with the experiments better than those of Ref. [17]. Contrary to proposal of the Ref. [17], attempting to explain the zero-bias anomaly in Co@Cu(100) as the results of inelastic spin excitations, our theory demonstrates that they can be better explained from the point of view of the "Kondo" physics.

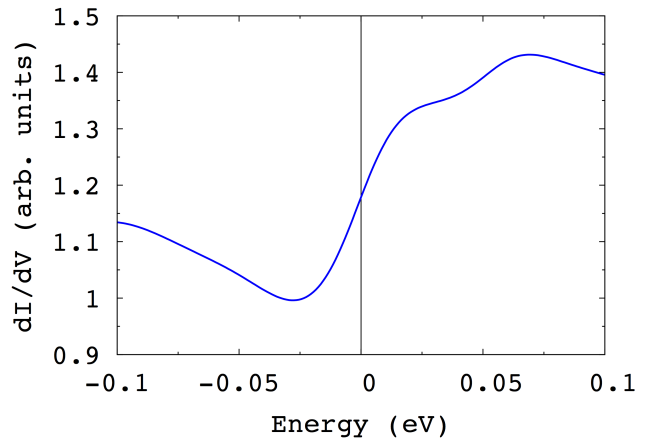


FIG. 4: Differential conductance \mathcal{G} calculated making use of the Eq.(6).

IV. SUMMARY

The many-body calculations within the multi-orbital SIAM for the Co adatom on the Cu(100) surface are performed. DFT calculations were used to define the input for the discrete bath model of forty bath orbitals, and the SOC included. We found that the peak in the DOS at E_F can occur for the Co atom d -shell occupation $n_d \approx 8$, and is connected to quasi-degenerate ground state of the SIAM. Without SOC, the lowest energy state is an effective $S = 1/2$ -like doublet, and next to it there is an effective $S = 1$ -like triplet, so the resonance in the DOS(E_F) does not represent a Kondo resonance. When SOC is included, the triplet states are split like $|J = 1, J_z\rangle$ eigenstates in a presence of the magnetic anisotropy $\hat{H}_{MA} = D\hat{J}_z^2$, so that the $|J = 1, J_z = 0\rangle$ singlet becomes a ground state. The corresponding DOS(E_F) peak corresponds to the Kondo resonance. This solution is verified by comparison with experimentally observed zero-bias anomaly in the differential conductance. Our calculations illustrate the essential rôle which the SOC, and corresponding uniaxial magnetic anisotropy, is playing in a formation of Kondo singlet in the multi-orbital low-dimensional systems.

V. ACKNOWLEDGMENTS

Financial support was provided by Operational Programme Research, Development and Education financed by European Structural and Investment Funds and the Czech Ministry of Education, Youth and Sports (Project No. SOLID21 - CZ.02.1.01/0.0/0.0/16_019/0000760), and by the Czech Science Foundation (GACR) grant No. 21-09766S. The work of A.I.L. is supported by European Research Council via Synergy Grant 854843 - FAST-CORR.

Appendix A: Fitting the bath hybridization

With the specific choice of the Cartesian reference frame (see Fig. 1), the local Green's function $G_0(z)$ becomes diagonal in the basis of cubic harmonics $m = \{xz, yz, xy, x^2 - y^2, 3z^2 - r^2\}$. Moreover, it is convenient to use the imaginary energy axis over the Matsubara frequencies $i\omega_n$. The corresponding non-interacting Green's function of the Eq.(1) will then become

$$G_{0,m}(i\omega_n) = \frac{1}{i\omega_n - \epsilon_m - \Delta_m(i\omega)},$$

with the hybridization function

$$\Delta_m(i\omega_n) = i\omega_n - \epsilon_m - G_{0,m}^{-1}(i\omega_n). \quad (\text{A1})$$

Thus, the hybridization function Eq. (A1) can be evaluated making use of the local Green's function $G_0(z)$. The discrete bath model is built by finding bath energies and amplitudes which reproduce the continuous hybridization function as closely as possible.

$$\tilde{\Delta}_m(i\omega_n) = \sum_{k=1}^K \frac{V_{km}^2}{i\omega_n - \epsilon_{km}}. \quad (\text{A2})$$

The fitting is done by minimizing the residual function,

$$f_m(\{\epsilon_{km}, V_{km}\}) = \sum_{n=1}^{N_\omega} \frac{1}{\omega_n^\gamma} \left| \tilde{\Delta}_m(i\omega_n) - \Delta_m(i\omega_n) \right|^2, \quad (\text{A3})$$

using the limited-memory, bounded Broyden–Fletcher–Goldfarb–Shanno method [33, 34], with the parameters ϵ_{km} and V_{km} as variables. The factor $\frac{1}{\omega_n^\gamma}$ with $\gamma = 0.5$ is used to attenuate the significance of the higher frequencies.

TABLE IV: Values of the d shell Δ_{CF} (eV), the bath energies ϵ_m^k (eV), and hybridisation parameters V_m^k (eV) evaluated from LDA .

m	xz	yz	xy	$x^2 - y^2$	$3z^2 - r^2$
Δ_{CF}	-0.043	-0.043	0.117	0.053	-0.082
$\epsilon_{k=1,m}$	-2.16	-2.16	-1.99	-2.01	-2.57
$V_{k=1,m}$	0.85	0.85	0.65	0.65	0.72
$\epsilon_{k=2,m}$	-0.08	-0.08	0.001	-0.02	-0.05
$V_{k=2,m}$	0.18	0.18	0.08	0.10	0.13
$\epsilon_{k=3,m}$	0.51	0.51	1.45	0.53	0.43
$V_{k=3,m}$	0.36	0.36	0.55	0.34	0.32
$\epsilon_{k=4,m}$	7.56	7.56	7.80	8.16	7.72
$V_{k=4,m}$	2.08	2.08	2.12	1.78	1.70

Appendix B: DOS as a function of μ for Co on Cu(001)

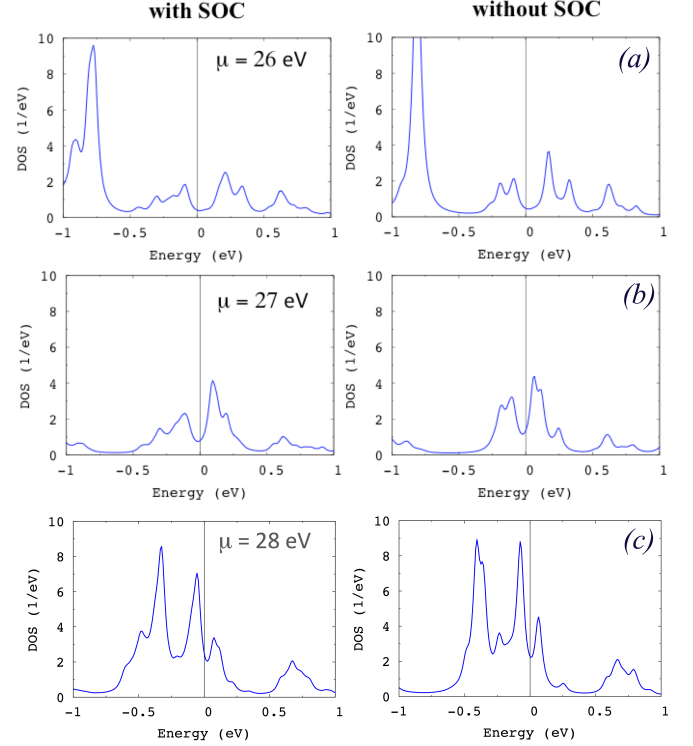


FIG. 5: DOS for the Co@Cu(001) with and without SOC as a function of $\mu = 26$ eV (a), 27 eV (b), and 28 eV (c)

-
- [1] G. D. Mahan, *Many-particle physics* (Springer Science & Business Media, Boston, MA, 2000).
 - [2] P. Monod, Phys. Rev. Lett. **19**, 1113 (1967).
 - [3] N. Knorr, M. A. Schneider, L. Diekhöner, P. Wahl and K. Kern , Phys. Rev. Lett. **88**, 096804 (2002).
 - [4] A. Zhao, Q. Li, L. Chen, H. Xiang, W. Wang, S. Pan, B. Wang, X. Xiao, J. Yang , J. Hou *et al.*, *Science* **309**, 1542 (2005).
 - [5] A. Abrikosov, Phys. Phys. Fiz. **2**, 5 (1965).
 - [6] H. Suhl, Phys. Rev. **138**, A515 (1965).
 - [7] Y. Nagaoka, Phys. Rev. **138**, A1112 (1965).
 - [8] P. Wahl, L. Diekhöner, M. A. Schneider, L. Vitali, G. Wittich and K. Kern, Phys. Rev. Lett. **93**, 176603 (2004).
 - [9] B. Surer, M. Troyer, P. Werner, T. O. Wehling, A. M. Läuchli , A. Wilhelm and A. I. Lichtenstein, Phys. Rev. B **85**, 085114 (2012).
 - [10] A. Valli, M. P. Bahlke, A. Kowalski, M. Karolak, C. Herrmann and G. Sangiovanni, Phys. Rev. Res. **2**, 033432 (2020).
 - [11] U. Fano, *Phys. Rev.* **124** 1866 (1961).
 - [12] A. N. Rubtsov , V. V. Savkin and A. I. Lichtenstein, Phys. Rev. B **72**, 035122 (2005).
 - [13] A. C. Hewson *The Kondo Problem to Heavy Fermions*, (Cambridge University Press, Cambridge, 1993)
 - [14] P. Hohenberg and W. Kohn, Phys. Rev. **136**, B864 (1964).
 - [15] N. Parragh, A. Toschi, K. Held and G. Sangiovanni, Phys. Rev. B **86**, 155158 (2012).
 - [16] M. Wallerberger, A. Hausoel, P. Gunacker, A. Kowalski, N. Parragh, F. Goth, K. Held and G. Sangiovanni, Computer Physics Communications **235**, 388 (2019).
 - [17] J. Bouaziz, F. S. M. Guimarães and S. Lounis, Nat. Commun. **11**, 1 (2020).
 - [18] G. Kresse and J. Furthmüller , Comput. Mater. Sci. **6**, 15 (1996).
 - [19] A. Georges, G. Kotliar, W. Krauth and M. J. Rozenberg, Rev. Mod. Phys. **68**, 13 (1996).
 - [20] A. I. Lichtenstein and M. I. Katsnelson, Phys. Rev. B **57**, 6884 (1998).
 - [21] E. Wimmer, H. Krakauer, M. Weinert and A. J. Freeman, Phys. Rev. B **24**, 864 (1981).
 - [22] W. Mannstadt and A. J. Freeman, Phys. Rev. B **55**, 13298 (1997).
 - [23] D. Jacob, J. Phys.: Condens. Matter **27**, 245606 (2015).
 - [24] A. MacDonald, W. Pickett and D. Koelling , J. Phys. C: Solid State Phys. **13**, 2675 (1980).
 - [25] M. Tchaplanka, A. B. Shick, J. Koloenc, J. Phys.: Conf. Ser. **2164**, 012045 (2022).
 - [26] K. Yosida, Phys. Rev. **147**, 223 (1966).
 - [27] V. I. Anisimov, J. Zaanen and O. K. Andersen, Phys. Rev. B **44**, 943 (1991).
 - [28] I. V. Solovyev, P. H. Dederichs and V. I. Anisimov, Phys. Rev. B **50**, 16861 (1994).
 - [29] M. Tchaplanka, A. Shick and A. Lichtenstein, New J. Phys. **23**, 103037 (2021).
 - [30] K. R. Patton, S. Kettmann, A. Zhuravlev and A. Lichtenstein Phys. Rev. B **76**, 100408(R) (2007).
 - [31] T. O. Wehling, H. P. Dahal, A. I. Lichtenstein, M. I. Katsnelson, H. C. Manoharan and A. V. Balatsky , Phys. Rev. B **81**, 085413 (2010).
 - [32] G. Bergmann, Phys. Rev. Lett. **57**, 1460 (1986).
 - [33] C. Zhu, R. H. Byrd , P. Lu and J. Nocedal, ACM Trans. Math. Software **23**, 550 (1997).
 - [34] J. L. Morales and J. Nocedal, ACM Trans. Math. Software **38**, 1 (2011).